New Journal of Physics
The open-access journal for physics

Positioning of microtubule organizing centers by cortical pushing and pulling forces

Nenad Pavin[1,2,5], Liedewij Laan[3,5,6], Rui Ma[1,4], Marileen Dogterom[3,7] and Frank Jülicher[1,7]

[1] Max Planck Institute for the Physics of Complex Systems (MPI-PKS), Dresden, Germany
[2] Department of Physics, Faculty of Science, University of Zagreb, Zagreb 10002, Croatia
[3] FOM Institute AMOLF, Science Park 104, 1098-XG Amsterdam, The Netherlands
[4] Institute for Advanced Study, Tsinghua University, Beijing 100084, China
E-mail: dogterom@amolf.nl and julicher@pks.mpg.de

New Journal of Physics **14** (2012) 105025 (13pp)
Received 6 July 2012
Published 29 October 2012
Online at http://www.njp.org/
doi:10.1088/1367-2630/14/10/105025

Abstract. Positioning of microtubule (MT) organizing centers with respect to the confining geometry of cells depends on pushing and/or pulling forces generated by MTs that interact with the cell cortex (Dogterom *et al* 2005 *Curr. Opin. Cell Biol.* **17** 67–74). How, in living cells, these forces lead to proper positioning is still largely an open question. Recently, it was shown by *in vitro* experiments using artificial microchambers that in a square geometry, MT asters center more reliably by a combination of pulling and pushing forces than by pushing forces alone (Laan *et al* 2012a *Cell* **148** 502–14). These findings were explained by a physical description of aster mechanics that includes slipping of pushing MT ends along chamber boundaries. In this paper, we extend that theoretical work by studying the influence of the shape of the confining geometry on the positioning process. We find that pushing and pulling forces can have centering or off-centering behavior in different geometries. Pushing forces center in a one-dimensional and a square geometry, but lead to off-centering in a circle

[5] These authors contributed equally to this paper.
[6] Present address: Faculty of Arts and Sciences Center for Systems Biology, Harvard University, Cambridge, USA.
[7] Authors to whom any correspondence should be addressed.

if slipping is sufficiently pronounced. Pulling forces, however, do not center in a one-dimensional geometry, but improve centering in a circle and a square. In an elongated stadium geometry, positioning along the short axis depends mainly on pulling forces, while positioning along the long axis depends mainly on pushing forces. Our theoretical results suggest that different positioning strategies could be used by different cell types.

Contents

1. Introduction

In cells, dynamic microtubules (MTs), organized in higher-order structures such as MT asters or MT bundles, exert forces on MT organizing centers (MTOCs). Such forces are important for the positioning of these organizing centers with respect to the periphery of the cell. In the fission yeast *Schizosaccharomyces pombe* for example, MTs organized in antiparallel bundles position the nucleus in the center by growth-based pushing forces generated at the cell poles (Tran *et al* 2001). The mechanism by which pushing forces position the nucleus has been studied quite extensively *in vivo* and *in vitro*, as well as theoretically (Holy *et al* 1997, Dogterom and Yurke 1998, Tran *et al* 2001, Faivre-Moskalenko and Dogterom 2002, Tolic-Norrelykke *et al* 2004). In many other systems however, positioning processes such as the centering of MT asters and the orientation of the mitotic spindle (Dujardin and Vallee 2002, Vallee and Stehman 2005, O'Connell and Wang 2000) have been suggested to rely on pulling forces generated at MT contacts with the cell cortex (Busson *et al* 1998, Koonce *et al* 1999, Burakov *et al* 2003). Pulling forces are also implicated in processes where the positioning needs to be asymmetric. In *Caenorrhabditis elegans* for example, MT-based pulling forces contribute to the asymmetric positioning of the mitotic spindle (Grill *et al* 2001). It is generally assumed that in this and other cases, the pulling force is mediated by the minus end-directed motor protein dynein that is linked to the cell cortex (Gonczy *et al* 1999). It has been proposed that, in addition, pulling forces may be generated by dynein along MTs in the cytoplasm (Hamaguchi and Hiramoto 1986, Kimura and Onami 2005, Wuhr *et al* 2010, Kimura and Kimura 2011a), which in particular may be relevant for large embryonic cells where MT asters need to position themselves without directly contacting the cell periphery (e.g. Wuhr *et al* 2009).

Several models have been proposed that describe the role of pulling forces in cellular positioning processes. In one of the earlier models, the positioning mechanism relies on the length dependence of pulling forces due to lateral interactions of force generators along the length of MTs (Hamaguchi and Hiramoto 1986, Zhu *et al* 2010, Kimura and Kimura 2011b), either at

the cortex or in the cytoplasm. In a more recent model, positioning relies on the assumption that only a small fraction of MTs interacting with the cortex is subject to pulling forces (Grill and Hyman 2005). However, for the general situation of length-independent cortical pulling forces that are not limited by the number of interaction sites, simple arguments based on the expected length distribution of dynamic MTs predict that MTOCs should not center: in response to cortical pulling forces, MT asters should move away from the center toward nearby boundaries where most cortical contacts are made, in contrast to the situation where pushing forces are generated (Hamaguchi and Hiramoto 1986, Dogterom *et al* 2005, Howard 2006).

At odds with this simple prediction, we have shown recently that in minimal *in vitro* experiments, cortical pulling forces in combination with pushing forces can in fact lead to efficient positioning of MT asters (Laan *et al* 2012a). These experiments were set up as follows: an MT aster was grown from an MTOC, a centrosome, in a square microfabricated chamber (Holy *et al* 1997, Faivre-Moskalenko and Dogterom 2002). A gold layer that was sandwiched in the sidewalls of the microfabricated chamber allowed for specific binding of biotinylated dynein molecules via gold-specific chemistry and biotin–streptavidin linkage (Romet-Lemonne *et al* 2005). Pushing forces arose from MT polymerization and buckling forces (Dogterom *et al* 2005, Howard 2006), and pulling forces arose from interactions between MT ends and the dynein motor proteins. We found that MT asters center more reliably by a combination of pulling and pushing forces than by pushing forces alone, provided that most MTs reach the periphery of the chamber. At first sight this was surprising. As depicted in figure 1(a), the net pulling forces on an MT aster that grows from an MTOC in an isotropic manner, located at any location in the confining space, is expected to be zero. To explain our data, we developed a theoretical description based on the following mechanism: slipping of pushing MTs along the chamber walls generates an anisotropic distribution of MTs that, once MT ends are captured by dynein, leads to a reliable centering force on the MT aster (figure 1(b)). We applied this model to the square geometry relevant to our *in vitro* experiments and showed that pulling forces indeed improve positioning of an MT aster.

In this paper, we extend our recent work by studying the general role of the geometry of the confining space in positioning processes driven by a combination of cortical pushing and pulling forces. Cells have different sizes and shapes and it is thus important to explore the general applicability of the positioning mechanism that we propose. We find that the magnitude as well as the direction of positioning forces differ in various geometries. Pushing forces center reliably in a one-dimensional geometry, but in the case of considerable slipping they lead to off-centering in a circular geometry. Pulling forces, however, do not lead to centering in a one-dimensional geometry but center in a circular and a square geometry. In elongated geometries, such as a stadium and a rectangle, we find that centering by pulling forces is more efficient along the short axis than along the long axis, as expected from an intermediate between a circle/square and a one-dimensional geometry. Our results suggest that different positioning strategies could be employed in different types of cells.

2. Physical description of a microtubule aster within a two-dimensional confinement

In our description of an MT aster, MTs radiate from an MTOC with position $\mathbf{r}$ (figure 1(c)). As in Laan *et al* (2012a), we consider two populations of MTs that are in contact with a boundary of a confining space: (i) pushing MTs distributed with angular density $n^+(\phi, t)$ and (ii) pulling MTs distributed with angular density $n^-(\phi, t)$, which are bound to dynein. Here ϕ describes

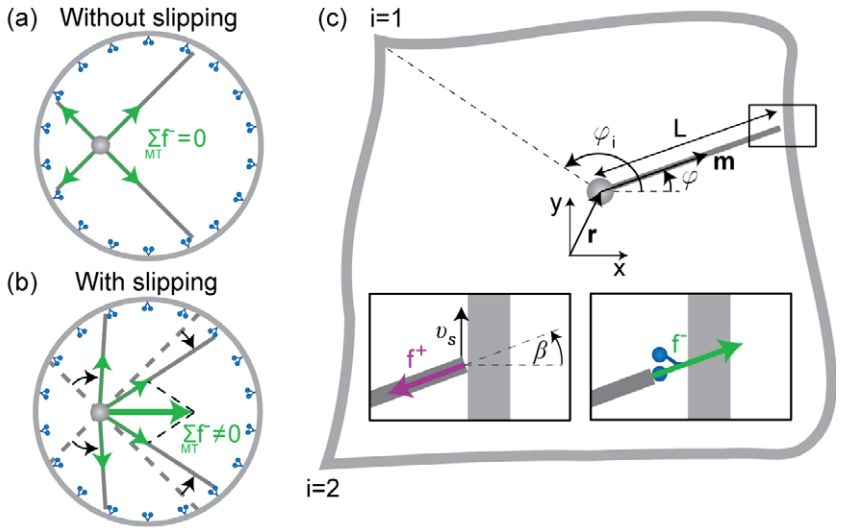

Figure 1. A model for centering due to slipping and pulling. (a), (b) Net pulling forces in a circular geometry. MTs and the MTOC are drawn in gray and motors are drawn in blue. (a) If there is no slipping, the MT distribution is isotropic, and the sum over all pulling forces on the MTOC is zero. (b) If MTs are slipping along the cell boundary, the MT distribution becomes anisotropic and the sum over all pulling forces on the MTOC is no longer zero. (c) Schematic representation of an MTOC at $\mathbf{r} = (x, y)$ in an arbitrary confining geometry, introducing the parameters used in our theoretical description of aster positioning. The MT orientation is described by the angle φ. The position of corner i is φ_i and L denotes the MT length. The left inset shows an MT under pushing force f^+, which slips along the wall with velocity υ_s. The angle between the MT orientation and the normal to the boundary is β. The right inset shows an MT under pulling force f^-.

the MT orientation relative to the x-direction and t denotes time. These MT distributions obey the following equations:

$$\frac{\partial n^+}{\partial t} = \frac{\nu}{2\pi} - k_{\mathrm{cat}} n^+ - k_{\mathrm{b}} n^+ - \frac{\partial}{\partial \phi} J_\phi, \tag{1}$$

$$\frac{\partial n^-}{\partial t} = k_{\mathrm{b}} n^+ - k_{\mathrm{off}} n^-. \tag{2}$$

Here, ν denotes the nucleation rate of MTs at the MTOC (note that we assume that all nucleated MTs reach the boundary instantly), k_{cat} denotes the catastrophe rate of pushing MTs, k_{b} denotes the rate of MT binding to dynein and k_{off} denotes the detachment rate of pulling MTs. The current

$$J_\phi = \upsilon_\phi n^+ \tag{3}$$

describes the reorientation of pushing MTs due to slipping along the boundary. In a situation where $\mathbf{r}$ is fixed, $\upsilon_\phi = (\upsilon_{\mathrm{s}}/L)\cos\beta$ is the rate of angular MT reorientation, where $L(\mathbf{r}, \phi)$ is the distance between the organizing center at $\mathbf{r}$ and the MT contact with the boundary, and $\beta(\mathbf{r}, \phi)$ is the angle between the MT orientation and the normal to the boundary. The slipping velocity

is $v_s = (f^+/\xi)\sin\beta$, where f^+ denotes the force exerted by a pushing MT on the boundary in the direction given by the MT, and ξ is the friction coefficient associated with slipping. Note that the function $\beta(\mathbf{r})$ can exhibit discontinuities, for example, if the geometry has corners. Such discontinuities occur at a discrete set of angles ϕ_i, $i = 1, \ldots, i_{\max}$ (figure 1(c)), where the slipping velocity, $v_\phi(\phi)$, is discontinuous, i.e. $v_i^+ \neq v_i^-$, where $v_i^\pm = \lim_{\varepsilon\to 0^+} v_\phi(\phi_i \pm \varepsilon)$. Thus, in geometries where such discontinuities occur, we describe the corresponding angles, which in the present work correspond to corners, separately. The theoretical description differs for cases in which MTs are slipping toward or away from the corners. If MTs are slipping toward a corner from both sides ($v_i^- > 0$ and $v_i^+ < 0$), they will get trapped there. In this case, we consider the numbers $N_i^+(t)$ and $N_i^-(t)$ of pushing and pulling MTs at $\phi = \phi_i(\mathbf{r})$. The MT numbers in that corner satisfy

$$\frac{\mathrm{d}N_i^+}{\mathrm{d}t} = J_i^- - J_i^+ - k_{\mathrm{cat}}N_i^+ - k_{\mathrm{b}}N_i^+, \tag{4}$$

$$\frac{\mathrm{d}N_i^-}{\mathrm{d}t} = k_{\mathrm{b}}N_i^+ - k_{\mathrm{off}}N_i^-. \tag{5}$$

Here, $J_i^\pm = \lim_{\varepsilon\to 0^+} J_\phi(\phi_i \pm \varepsilon)$ are MT currents leaving/entering the corners from both sides. If MTs, however, are slipping away from a corner from one side and toward that corner from the other side ($v_i^-, v_i^+ > 0$ or $v_i^-, v_i^+ < 0$), the same number of MTs is leaving/entering that corner, $J_i^- = J_i^+$. Finally, if MTs are slipping away from a corner from both sides ($v_i^- < 0$ and $v_i^+ > 0$), the density at $\phi = \phi_i$ vanishes: $n^+(\phi_i \pm \varepsilon) = 0$ for $\varepsilon \to 0^+$.

The net force acting on the organizing center is given by $\mathbf{F} = \mathbf{F}^+ + \mathbf{F}^-$, where

$$\mathbf{F}^\pm = \mp \int_0^{2\pi} \mathrm{d}\phi n^\pm f^\pm \mathbf{m} \mp \sum_{i=1}^{i_{\max}} N_i^\pm f^\pm \mathbf{m} \tag{6}$$

correspond to the net pushing and pulling forces, respectively. Here, $\mathbf{m}(\phi)$ denotes the unit vector in the direction of the MT at an angle ϕ. The pushing force of a single MT is assumed to be limited by MT buckling, which is described by the Euler buckling formula $f^+ = \pi^2\kappa/L^2$, where κ denotes the MT bending rigidity (Gittes *et al* 1993). In addition, the pushing force may be limited by the MT polymerization force that is related to the polymerization velocity (Dogterom and Yurke 1997). This limit becomes relevant only for MTs that are very short (and therefore the Euler buckling force exceeds the so-called stall force at which MTs can no longer grow), or in general when the polymerization velocity is significantly smaller than the predicted slipping velocity. For a typical force of 3 pN (corresponding the buckling force of an MT with a length of about 10 μm) and a friction coefficient of $\xi = 50\,\mathrm{pN\,s\,\mu m^{-1}}$, the slipping velocity is predicted to be $0.06\,\mu\mathrm{m\,s^{-1}}$, which is of the same order as the MT growth velocity (several $\mu\mathrm{m\,min^{-1}}$). Therefore, for the sake of simplicity, we assume the pushing force to be limited by Euler buckling. The pulling force $f^- > 0$ is considered to be constant. In the steady state, $\partial_t n^+ = \partial_t n^- = 0$. If the total number of MTs, M, contacting the boundary is imposed, the nucleation rate becomes $\nu = M\,(k_{\mathrm{cat}} + k_{\mathrm{b}})\,/\,(1 + k_{\mathrm{b}}/k_{\mathrm{off}})$, where $M = \int_0^{2\pi}\mathrm{d}\phi\left(n^+ + n^-\right) + \sum_i\left(N_i^+ + N_i^-\right)$ is the total number of MTs in contact with the boundary. Note that in our calculation of static forces on MTOCs at fixed positions, we do not explicitly account for length changes of MTs due to (force-dependent) growth or shrinking (Dogterom and Yurke 1997, Janson and Dogterom 2004), nor do we account for any tilting of MT ends due to buckling of pushing MTs. In this simplest description we consider MTs to remain straight.

Table 1. Parameter choices.

Parameter	Value	Based on
M	$= 50$MTs	Rough estimate from experiments where MTs were grown from centrosomes under similar experimental conditions
k_{cat}	$= 10^{-2}\,\text{s}^{-1}$	Estimated from the dynamics of MTs in the microfabricated chambers
k_{off}	$= 10^{-2}\,\text{s}^{-1}$	Rough estimate from Laan *et al* (2012a) and from the dynamics of the MTs in the microfabricated chambers
k_{b}	$= 10^{-2}\,\text{s}^{-1}$	Equal to k_{off}
f^-	$= 5\,\text{pN}$	Taken from Laan *et al* (2012a) and Gennerich *et al* (2007))
ξ	$= 50\,\text{pN}\,\text{s}\,\mu\text{m}^{-1}$	Rough estimate from experiments on MTs growing from centrosomes attached to the surface against the gold barrier coated with dynein
κ	$= 33.12\,\text{pN}\,\mu\text{m}^2$	Taken from Gittes *et al* (1993)

3. Positioning in two-dimensional versus one-dimensional geometries

To investigate the positioning mechanism in different geometries, we compared the calculated MT distributions and the corresponding forces in a circular geometry, a square geometry and a one-dimensional elongated geometry. We chose the parameters to be essentially the same as those in our previous study (Laan *et al* 2012a). However, we chose k_{b} to be equal to k_{off} in order to compare forces generated by the same number of pushing and pulling MTs (table 1). In a circular geometry, pushing MTs slip along the boundary and this leads to an accumulation of MTs on the side of the chamber opposite to the direction in which the aster is displaced (figure 2(a)). We refer to this opposite side as the distal side. When many MTs are contacting the distal side compared to MTs contacting the proximal side, pushing forces can become off-centering (despite the fact that long MTs exert smaller forces than short ones due to MT buckling, as described by the Euler buckling formula). This happens when the friction coefficient ξ is sufficiently small, and therefore slipping distances become sufficiently large (figure 2(b), magenta curve). In contrast, at high friction coefficient, slipping distances are reduced and the MT anisotropy is weak. In this case pushing forces have a centering effect due to the length dependence of the buckling force (figure 2(c), magenta curve). Pulling forces, on the other hand, always contribute a centering force, although the magnitude of the net pulling force is reduced for increased friction ξ (figures 2(b) and (c), green curves). In a square geometry, the MT anisotropy is more pronounced than in a circular geometry for the same set of parameter values (compare figures 2(a) and (d)). However, the magnitude of the net pulling force is smaller in a square geometry than in a circle (compare figures 2(b), (c) and 2(e), (f)). This difference is related to the fact that in a circular geometry all MTs slip in the distal direction, whereas in a square geometry some of the MTs slip in the opposite direction. As a consequence, centering by pulling forces is more reliable in a circular geometry than in a square geometry. Recall that for the same reason, centering by pushing is less reliable in a circular geometry than in a square geometry. Interestingly, in a one-dimensional geometry the situation is very different: slipping cannot occur at all (figure 2(g)) and pushing forces always center (figure 2(h), magenta curve) as previously described (Dogterom and Yurke 1998, Dogterom *et al* 2005, Howard 2006).

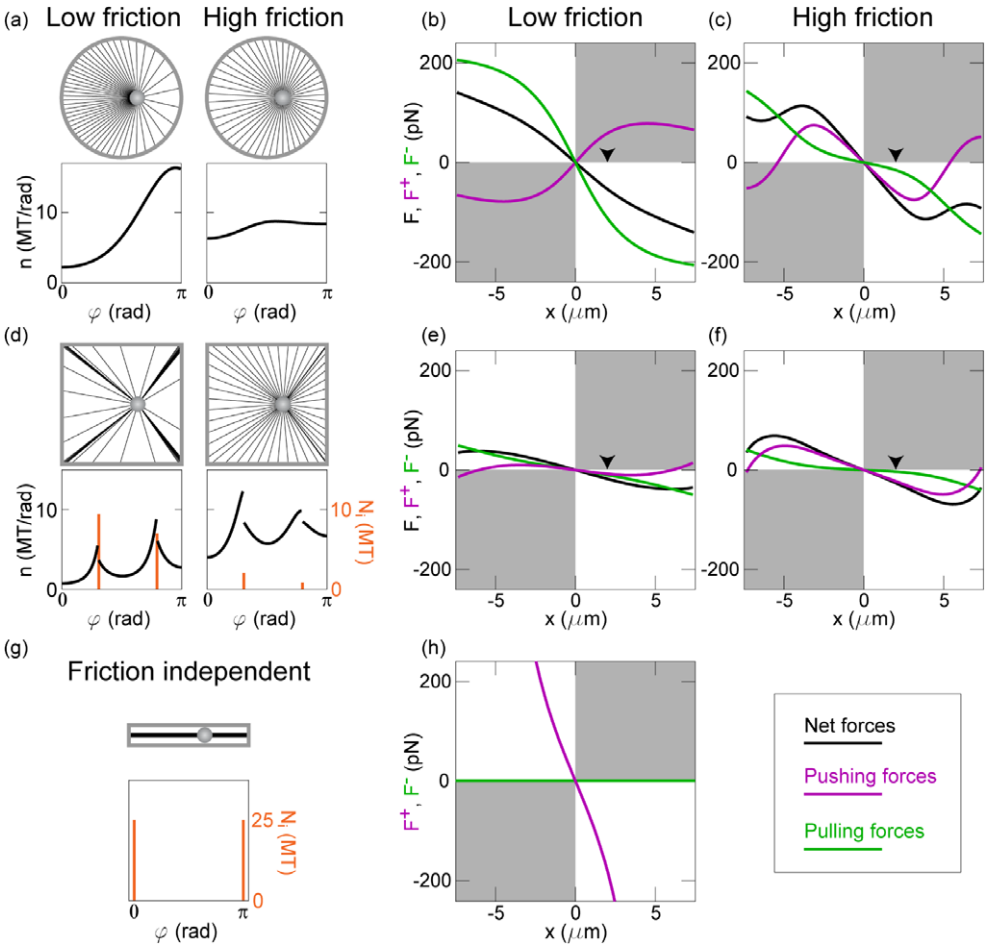

Figure 2. MT distributions and forces in a circle, a square and a one-dimensional geometry. For different geometries the MT distribution, $n = n^+ + n^-$, is shown for an MTOC 2 μm displaced from the center in a geometry with a width of 15 μm, and $N_i = N_i^+ + N_i^-$ is the total number of MTs at corner ϕ_i (orange bars). The net (black), pulling (green) and pushing (magenta) forces on the MTOC are plotted for different positions along the x-axis, x, in the geometry. The black arrowheads indicate the 2 μm displacement used for the MT distributions. The white quadrants show centering forces and the gray quadrants show off-centering forces. (a) MT distributions in a circular geometry, for two different values of the friction: low friction $\xi = 10^{-5}\,\mathrm{N\,s\,m^{-1}}$ and high friction $\xi = 10^{-4}\,\mathrm{N\,s\,m^{-1}}$. (b), (c) Net pulling and pushing forces for two different ξ in a circular geometry. (d) MT distributions in a square geometry, for two different ξ. (e), (f) Net pulling and pushing forces for two different ξ in a square geometry. (g) In a one-dimensional geometry we define two populations of MTs. These populations contain equal numbers of MTs, but with orientations in opposite directions. Note that in this geometry MTs do not change their initial orientation by slipping and thus MT distributions are friction independent. (h) Net pulling and pushing forces for a one-dimensional geometry. The parameters used in these graphs are $k_{\mathrm{cat}} = 10^{-2}\,\mathrm{s^{-1}}$, $k_{\mathrm{b}} = 10^{-2}\,\mathrm{s^{-1}}$, $k_{\mathrm{off}} = 10^{-2}\,\mathrm{s^{-1}}$, $f^- = 5\,\mathrm{pN}$, $\kappa = 3.3 \times 10^{-23}\,\mathrm{N\,m^2}$, $M = 50$.

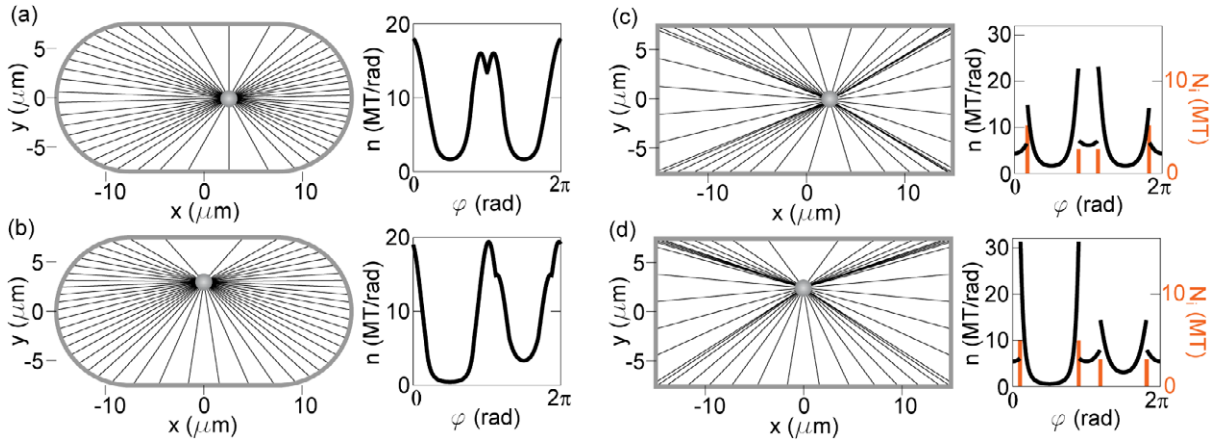

Figure 3. MT distributions in a stadium and a rectangle. For the different geometries the MT distributions are shown in a geometry with a length of 30 μm and a width of 15 μm. (a), (b) MT distributions in a stadium geometry, where the MTOC is 2.5 μm displaced from the center, along the x-axis (a) and along the y-axis (b) with low friction $\xi = 10^{-5}\,\mathrm{N\,s\,m^{-1}}$. (c), (d) MT distributions in a rectangular geometry with the MTOC 2.5 μm displaced from the center along the x-axis (c) and y-axis (d), for low friction. The remaining parameters used in these graphs are the same as in figure 2.

This is in contrast to pulling forces, which do not relay any positional information in this geometry (figure 2(h), green curve).

4. Positioning in elongated geometries

In the previous section, we have shown the opposite roles pushing and pulling forces can have in a circular versus a one-dimensional geometry. To understand how a transition between these two extremes occurs, we investigate positioning in two elongated geometries: in a stadium and in a rectangle. In figure 3, we plot MT distributions for an MTOC displaced from the center either along the long or the short axis, for both geometries (see figure 4 for the corresponding force fields). In all cases MTs tend to align with the long axis, resulting in the same number of MTs pointing to the left and to the right, similar to the one-dimensional case. Compared with displacement along the long axis (figures 3(a) and (c)), MT asymmetry is more pronounced for displacement along the short axis (figure 3(b) and (d)). For the stadium, this asymmetry is reflected by fewer MTs pointing upward, in the direction of the displacement, than downward, in the opposite direction (figure 3(b)). In a rectangle, MTs instead accumulate in the corners as they do in a square (figures 3(c) and (d)).

Forces experienced by the MTOC reflect the distribution of MTs. In all geometries, in the vicinity of the center, pulling forces are directed parallel to the short axis and are pointing toward the center (figures 4(a)–(d), top). This means that pulling forces have a centering character along the short axis, while along the long axis there is almost no positional information, similar to the one-dimensional case. To find the position of the force-balanced states along the long axis, we calculated pulling forces at smaller spacings than indicated in the figure. In a stadium

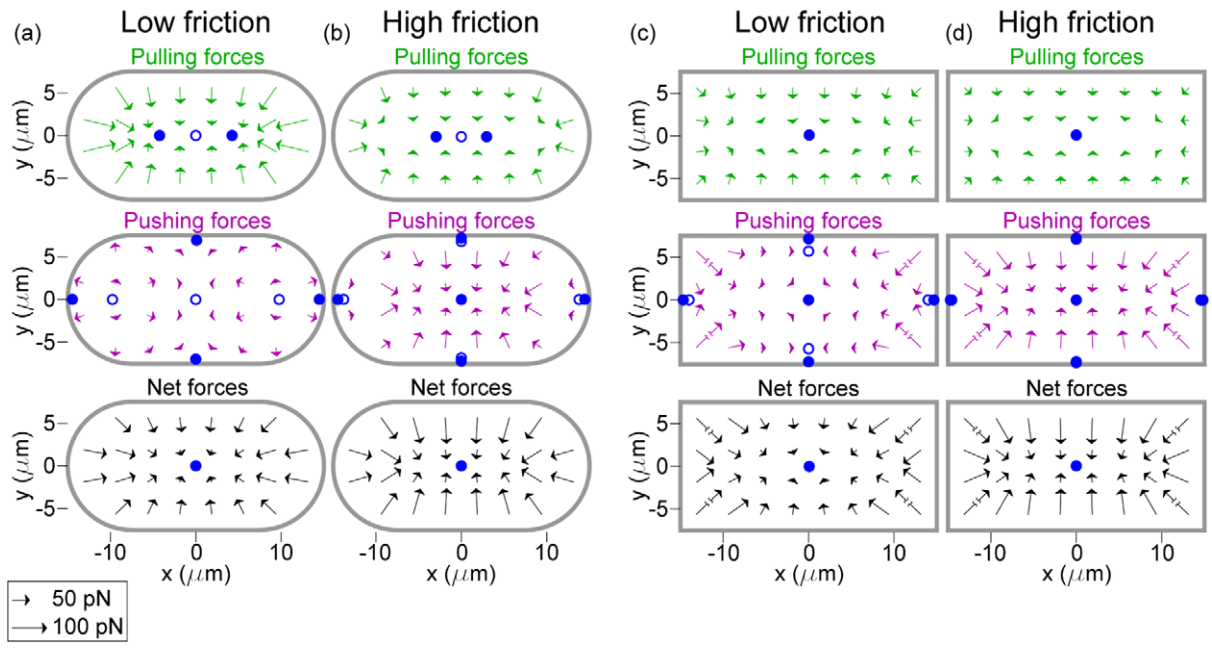

Figure 4. Force fields in a stadium and a rectangle. Force fields of the pulling (green), pushing (magenta) and net (black) forces in two different geometries with a length of 30 μm and a width of 15 μm. (a), (b) Force fields in a stadium geometry for two different frictions: low friction $\xi = 10^{-5}\,\mathrm{N\,s\,m^{-1}}$ and high friction $\xi = 10^{-4}\,\mathrm{N\,s\,m^{-1}}$. (c), (d) Force fields in a rectangular geometry, for two different ξ. The arrows representing the forces in the vicinity of corners are smaller (by about a factor of 3) than the actual (relative) magnitude of these forces and are thus crossed by two tildes. The remaining parameters used in these graphs are the same as in figure 2. Full and hollow blue circles show the stable and unstable force-balanced states, respectively. The force-balanced states are found by additional calculations of the forces along the long and short symmetry axes with a spacing of 0.15 μm.

(figures 4(a) and (b), top), we found an unstable force-balanced state at the center (open blue circle) and two stable force-balanced states in the vicinity of the center (solid blue circles). In a rectangle there is a single stable force-balanced state at the center (figures 4(c) and (d), top, solid blue circle). Away from the center, close to the poles, pulling forces are pointing toward the center irrespective of whether the displacement is along the long or short axis. For pushing forces, the result depends on the shape and on the magnitude of the friction coefficient (figures 4(a)–(d), middle). In a stadium at low friction, the pushing forces are, for small displacements, centering along the long axis and off-centering along the short axis, with an unstable force-balanced state at the center (figure 4(a), middle). In the remaining three cases, in a stadium at high friction and in a rectangle at both frictions, the pushing forces are centering along both the axes, resulting in a stable force-balanced state at the center (figures 4(b)–(d), middle). In all the cases, for the MTOC displaced far away from the center, four additional stable force-balanced states occur at the edges (figure 4, middle). In all the cases, the combined

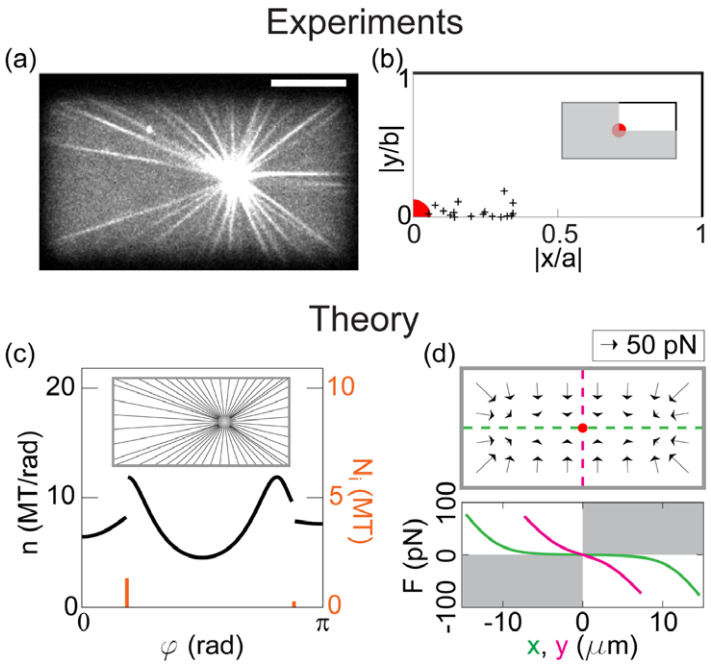

Figure 5. The positioning of MT asters in a rectangular geometry (experiment and theory). (a) Single plane spinning disc confocal fluorescence image of an MT aster in a rectangular microfabricated chamber. The scale bar is 10 μm. (b) Scatter plot of the absolute aster positions (pluses), normalized with the chamber half-length and half-width a and b. The ratio $a : b = 2 : 1$ is the same for all chambers. (c) Theoretical MT distribution in a rectangle with a length of 30 μm and a width of 15 μm as a function of ϕ for an MTOC 4 μm displaced from the center. (d) Vector field in which arrows indicate the net forces acting on the MTOC in a chamber due to cortical pushing and pulling forces. The full red circle shows the stable force-balanced state, and the dashed green and pink lines indicate the lines along which the forces are shown below. The parameters used in (c) and (d) are $\xi = 5 \times 10^{-5}\,\mathrm{N\,s\,m^{-1}}$, $k_{\mathrm{cat}} = 10^{-3}\,\mathrm{s^{-1}}$, $k_{\mathrm{b}} = 2 \times 10^{-2}\,\mathrm{s^{-1}}$, $k_{\mathrm{off}} = 10^{-4}\,\mathrm{s^{-1}}$. The remaining parameters are the same as in figure 2.

pushing and pulling forces are centering with stronger centering forces along the short axis as compared with the long axis (figure 4, bottom).

5. Comparison of experiments and theory of positioning in elongated geometries

To verify experimentally that MT asters indeed position more reliably along the short than the long axis of an elongated geometry, we performed *in vitro* experiments in rectangular microfabricated chambers with a length-to-width ratio of 2:1 (figure 4(a)). The length varied from 15 to 80 μm. The experiments were performed as described previously under the same experimental conditions (Laan and Dogterom 2010, Laan *et al* 2012a). In brief, dynein molecules were specifically bound to a 700 nm thick gold layer in the sidewalls of the microfabricated chambers. MT asters were grown at 25 °C with fluorescent tubulin (22 μM tubulin, 1.6 μM Rhodamin tubulin, cytoskeleton, and Denver) from centrosomes (purified from

human lymphoblastic KE37 cell lines), and imaged using spinning disc confocal (single plane) fluorescence microscopy. In figure 5(a) an experimental picture of an MT aster in a rectangular chamber is shown. The anisotropic MT distribution indicates the slipping of MTs along the chamber walls, which is supported by comparing the experimental data directly with the theoretical prediction (figure 5(c)). For this comparison the position $\mathbf{r}$ of the MTOC is chosen at the same location as in the experiment. The parameters in the model are chosen to match the experimental conditions (see the caption of figure 5). We studied the centering efficiency of MT asters by recording the positions of 17 asters. These asters had MTs that were all long enough to reach the edges of the microfabricated chamber and did not show observable movement (anymore). The relative positions of these asters in chambers of different sizes, normalized with the chamber half-width and half-length, are plotted in figure 5(b). This plot shows that deviations from the center along the y-axis, $y/b = 0 \pm 0.06$ (mean $\pm$ SD), are much smaller than deviations along the x-axis, $x/a = 0 \pm 0.24$ (mean $\pm$ SD), implying an eightfold better positioning along the short axis than the long axis, compared in absolute coordinates. Interestingly, our theory predicts that forces experienced by the MTOC at $\mathbf{r}_1 = (0.24a, 0)$ and $\mathbf{r}_2 = (0, 0.06b)$, positions that represent deviations along the x- and y-axis, respectively, are of comparable magnitudes $F(\mathbf{r}_1)/F(\mathbf{r}_2) \approx 0.57$. Both experimental and theoretical results thus suggest that positioning is more efficient along the short axis than along the long axis (figures 5(b) and (d)).

6. Discussion

Living cells have various sizes and shapes. For example, sea urchin eggs have spherical shapes. Mammalian cells obtain an elongated shape during cell division and cells within tissues often have polygonal shapes because they interact with neighboring cells. In all these cases the centrosome tends to be positioned near the cell center and the mitotic spindle is aligned with the long cell axis (O'Connell and Wang 2000, Minc *et al* 2011). Our findings show that cortical MT pulling forces together with MT slipping could explain the robust centering of MT asters in all these cell types. Further, our findings show that in elongated geometries, positioning along the short axis is more reliable than along the long axis, implying that two separate asters would distribute along the central part of the long axis. This could explain the alignment of mitotic spindles with the long axis of cells.

Recently, in a series of *in vivo* experiments, Minc and colleagues (Minc *et al* 2011) investigated the positioning of the nucleus in sea urchin eggs, which are of the order of 100 μm in size. These eggs were confined to microfabricated chambers of different geometries to change their shape accordingly. The position of the nucleus was found to be at the center of mass of the cell, independent of cell geometry. This result was explained by a theory based on the assumption that MT pulling forces are length dependent, similar to what has been proposed for large millimeter-size cells where MTs do not reach the cell cortex (Wuhr *et al* 2010). However, our theory based on length-independent cortical pulling forces could also explain the experimentally observed centering of the nucleus in a square and in elongated geometries as a result of MT slipping. Further *in vivo* experiments, in this and other systems, will be necessary to investigate the relative role of this slipping mechanism compared to centering due to length-dependent pulling forces. For example, in this study we predict that in elongated cells MTs tend to align with the long axis and that centering of the MTOC along the longer axis is less accurate than along the shorter axis. This prediction for elongated cells could be tested by measuring angular distributions of MTs and centrosome positions in experiments such as performed by

Minc and colleagues (Minc *et al* 2011). Alternatively, selective laser ablation of MTs at different distances from the centrosome, such as in Vogel *et al* (2009), may provide a direct answer to whether the pulling forces are generated along the MT lattice or at the MT ends.

In this study we have focused on static forces on MTOCs at a fixed position. Our results suggest that spontaneous redistribution of MT orientations due to slipping leads to an efficient centering strategy for dynamic MT asters subject to cortical pulling forces. In the future, it will be interesting to study, both experimentally and theoretically, the dynamic aspects of the positioning process. Experimentally perturbing the force balance with laser ablation (Grill *et al* 2001, Vogel *et al* 2009) should, for example, reveal whether the MT aster is indeed dynamically centered, and whether the subsequent dynamic response of the aster is consistent with a theoretical analysis of the dynamics of our system. We are furthermore extending both our experimental and theoretical work to three-dimensional geometries and asymmetric motor distributions, as well as to systems with soft deformable geometries bringing our analysis closer to the situation in cells. One might speculate that centering by slipping will be less efficient if the geometry is strongly deformable because the MTs will generate a local 'corner' which will prevent slipping and may even allow for lateral contacts (Laan *et al* 2012b). However, *in vitro* experiments as well as detailed calculations will be necessary to shed light on this problem.

Acknowledgments

We thank Bela Mulder and Iva Tolic-Norrelykke for discussions and a critical reading of the manuscript. NP acknowledges support from the Volkswagen Stiftung. RM thanks the China Scholarship Council (CSC) for a scholarship. LL and MD gratefully acknowledge the Human Frontier Science Program (HFSP) for funding. This work is part of the research program of the Foundation for Fundamental Research on Matter (FOM), which is part of the Netherlands Organisation for Scientific Research (NWO).

References

Burakov A, Nadezhdina E, Slepchenko B and Rodionov V 2003 Centrosome positioning in interphase cells *J. Cell Biol.* **162** 963–9

Busson S, Dujardin D, Moreau A, Dompierre J and De Mey J R 1998 Dynein and dynactin are localized to astral microtubules and at cortical sites in mitotic epithelial cells *Curr. Biol.* **8** 541–4

Dogterom M and Yurke B 1997 Measurement of the force–velocity relation for growing microtubules *Science* **278** 856–60

Dogterom M and Yurke B 1998 Microtubule dynamics and the positioning of microtubule organizing centers *Phys. Rev. Lett.* **81** 485–8

Dogterom M, Kerssemakers J W, Romet-Lemonne G and Janson M E 2005 Force generation by dynamic microtubules *Curr. Opin. Cell Biol.* **17** 67–74

Dujardin D L and Vallee R B 2002 Dynein at the cortex *Curr. Opin. Cell Biol.* **14** 44–9

Faivre-Moskalenko C and Dogterom M 2002 Dynamics of microtubule asters in microfabricated chambers: the role of catastrophes *Proc. Natl Acad. Sci. USA* **99** 16788–93

Gennerich A, Carter A P, Reck-Peterson S L and Vale R D 2007 Force-induced bidirectional stepping of cytoplasmic dynein *Cell* **131** 952–65

Gittes F, Mickey B, Nettleton J and Howard J 1993 Flexural rigidity of microtubules and actin filaments measured from thermal fluctuations in shape *J. Cell Biol.* **120** 923–34

Gonczy P, Pichler S, Kirkham M and Hyman A A 1999 Cytoplasmic dynein is required for distinct aspects of MTOC positioning, including centrosome separation, in the one cell stage *Caenorhabditis elegans* embryo *J. Cell Biol.* **147** 135–50

Grill S W and Hyman A A 2005 Spindle positioning by cortical pulling forces *Dev. Cell* **8** 461–5

Grill S W, Gonczy P, Stelzer E H K and Hyman A A 2001 Polarity controls forces governing asymmetric spindle positioning in the *Caenorhabditis elegans* embryo *Nature* **409** 630–3

Hamaguchi M S and Hiramoto Y 1986 Analysis of the role of astral rays in pronuclear migration in sand dollar eggs by the colcemid-UV method *Dev. Growth Differ.* **28** 143–56

Holy T E, Dogterom M, Yurke B and Leibler S 1997 Assembly and positioning of microtubule asters in microfabricated chambers *Proc. Natl Acad. Sci. USA* **94** 6228–31

Howard J 2006 Elastic and damping forces generated by confined arrays of dynamic microtubules *Phys. Biol.* **3** 54–66

Janson M E and Dogterom M 2004 Scaling of microtubule force–velocity curves obtained at different tubulin concentrations *Phys. Rev. Lett.* **92** 248101

Kimura A and Onami S 2005 Computer simulations and image processing reveal length-dependent pulling force as the primary mechanism for *C. elegans* male pronuclear migration *Dev. Cell* **8** 765–75

Kimura K and Kimura A 2011a Intracellular organelles mediate cytoplasmic pulling force for centrosome centration in the *Caenorhabditis elegans* early embryo *Proc. Natl Acad. Sci. USA* **108** 137–42

Kimura K and Kimura A 2011b A novel mechanism of microtubule length-dependent force to pull centrosomes toward the cell center *Bioarchitecture* **1** 74–9

Koonce M P, Kohler J, Neujahr R, Schwartz J M, Tikhonenko I and Gerisch G 1999 Dynein motor regulation stabilizes interphase microtubule arrays and determines centrosome position *EMBO J.* **18** 6786–92

Laan L and Dogterom M 2010 In vitro assays to study force generation at dynamic microtubule ends *Methods Cell Biol.* **95** 617–39

Laan L, Pavin N, Husson J, Romet-Lemonne G, van Duijn M, Lopez M P, Vale R D, Julicher F, Reck-Peterson S L and Dogterom M 2012a Cortical dynein controls microtubule dynamics to generate pulling forces that position microtubule asters *Cell* **148** 502–14

Laan L, Roth S and Dogterom M 2012b End-on microtubule–dynein interactions and pulling-based positioning of microtubule organizing centers *Cell Cycle* **11** 1–8

Minc N, Burgess D and Chang F 2011 Influence of cell geometry on division-plane positioning *Cell* **144** 414–26

O'Connell C B and Wang Y L 2000 Mammalian spindle orientation and position respond to changes in cell shape in a dynein-dependent fashion *Mol. Biol. Cell* **11** 1765–74

Romet-Lemonne G, VanDuijn M and Dogterom M 2005 Three-dimensional control of protein patterning in microfabricated devices *Nano Lett.* **5** 2350–4

Tolic-Norrelykke I M, Sacconi L, Thon G and Pavone F S 2004 Positioning and elongation of the fission yeast spindle by microtubule-based pushing *Curr. Biol.* **14** 1181–6

Tran P T, Marsh L, Doye V, Inoue S and Chang F 2001 A mechanism for nuclear positioning in fission yeast based on microtubule pushing *J. Cell Biol.* **153** 397–411

Vallee R B and Stehman S A 2005 How dynein helps the cell find its center: a servomechanical model *Trends Cell Biol.* **15** 288–94

Vogel S K, Pavin N, Maghelli N, Julicher F and Tolic-Norelykke I M 2009 Self-organization of dynein motors generates meiotic nuclear oscillations *PLoS Biol.* **7** e1000087

Wuhr M, Dumont S, Groen A C, Needleman D J and Mitchison T J 2009 How does a millimeter-sized cell find its center? *Cell Cycle* **8** 1115–21

Wuhr M, Tan E S, Parker S K, Detrich H W III and Mitchison T J 2010 A model for cleavage plane determination in early amphibian and fish embryos *Curr. Biol.* **20** 2040–5

Zhu J, Burakov A, Rodionov V and Mogilner A 2010 Finding the cell center by a balance of dynein and myosin pulling and microtubule pushing: a computational study *Mol. Biol. Cell* **21** 4418–27